INVESTIGATION THE EFFECT OF PARTICLE SIZE DISTRIBUTION ON PROCESSING PARAMETERS OPTIMISATION IN SELECTIVE LASER MELTING PROCESS

Bochuan Liu, Ricky Wildman, Christopher Tuck, Ian Ashcroft, Richard Hague

Additive Manufacturing Research Group, Loughborough University

Abstract

Selective Laser Melting is an efficient process for producing metal parts with minimal subtractive post-processing required. Analysis of the parameters controlling the part quality has been performed focussing on the energy intensity during processing and the effect of the particle size distribution on factors such as ultimate tensile strength and surface finish. It is shown that the controlling the energy intensity is key to quality and can be affected by varying, for example, laser beam diameter or the scanning rate.

Keywords: Particle size distribution; Powder bed; Processing parameters; Quality of finishing parts; Selective Laser Melting

1 Introduction

Selective laser melting (SLM) is a laser based additive manufacturing (AM) technique, which is able to build complex geometries directly from 3D CAD (computer-aided design) models, thereby allowing for great design freedom, and without the need of tooling [1-3]. As a process similar to laser sintering (LS), SLM uses a higher energy input to enable full melting of the powder bed materials, in order to build full dense parts without post-processing.

Optimal fabrication of parts using SLM requires a comprehensive understanding of the main processing parameters. In SLM, energy input, powder bed properties and build conditions are three leading factors that can affect the part's quality, which can be measured in various ways, including final part density, surface finishing and mechanical properties.

Laser energy density, E_ρ, is a key factor that affects the final part's quality in the SLM process to quantify energy input [1]. It is defined by the laser power, P (W), laser scanning speed, u (mm/s) and laser beam diameter, δ (mm) in the equation below.

$$E_\rho = \frac{P}{u\delta} \ (J/mm^2)$$

Powder bed properties, including bulk density and thermal properties, affect the final part properties. Powder particle size distribution plays an important role in sintering kinetics and powder bed formation [4, 5]. Investigations on the effect of particle size and size distribution have been carried out for sintering ceramics [6-8]. However, the effect of particle size distribution on laser sintering has not been well documented, especially in direct metal laser fabrication area [9, 10]. Also, investigations which compare the laser sintering behaviour of powders with similar average size, but different size distribution range are very limited.

In this paper, the effect of various process parameters, both relating to the powder and the laser properties, on final build quality is observed. In particular the effects on mechanical properties, which are ultimately what defines performance in use, are considered.

2 Experimental procedures

2.1 Initial characterisation

Two sets of gas atomised Stainless Steel 316L powders were obtained from two suppliers, Sandvik Osprey Ltd and LPW Technology Ltd. These were chosen for their similar chemical composition (data provided by the suppliers), but different particle size distribution (as measured by the suppliers). Supplier data indicated that Sandvik Osprey (SO) particle size was in the range 0-45µm and LPW Technology (LPW) in the range 15-45µm. Upon receipt, the powders were characterised in house using a LEO 440 Scanning Electron Microscope (SEM) and a Malvern Mastersizer 2000 laser diffraction based particle size analyser with a Scirocco dry dispersion accessory.

2.2 Powder bed density measurement

It is necessary to determine the powder bed density during the manufacturing process. To achieve this, a container was produced by SLM with internal dimensions of 30mm(X), 30mm(Y), 30mm(Z) (Figure.1). During the building process, the blade delivers the powder uniformly across the powder bed, but only the container is melted, leaving the unaffected powder within the container. After the build, the powder inside the box was weighed using a scale with an accuracy of 0.1mg and the packing density determined.
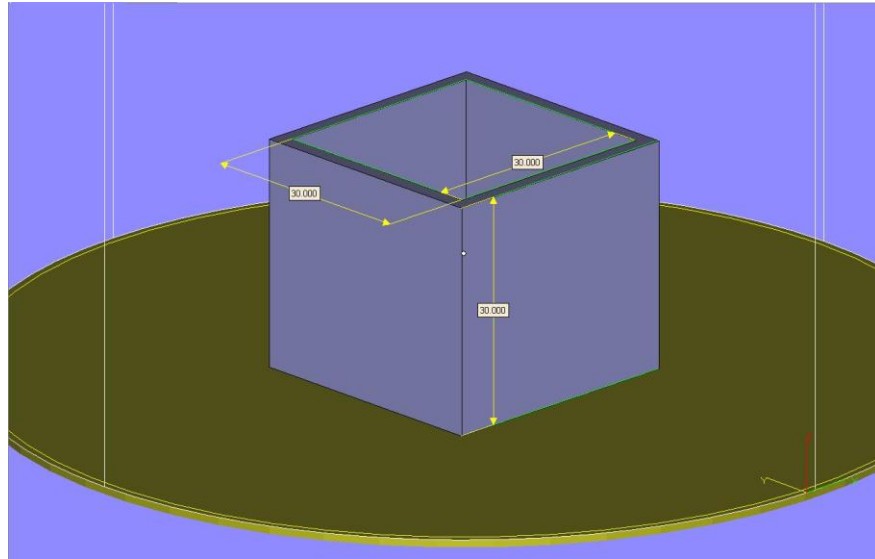
Figure.1 Design of container built for powder bed density measurement

2.3 Powder flowability measurement

The powder flowability is a powder characteristic which can affect the particle distribution on the powder bed, is itself affected by the powder particle size distribution. In SLM process, good powder flowability is required to achieve uniform thickness of powder layers, which allows uniform laser energy absorption in the processing area.

The Hausner ratio is a number which is correlated to the powder flowability. It is calculated using the equation shown below [11]:

$$H = \frac{\rho_T}{\rho_A}$$

where ρ_T is tapped density of powder, and ρ_A is apparent density of powder. A Hausner ratio greater than 1.25 is considered to be an indication of poor flowability [11]. Powder apparent and tapped densities were measured according to ASTM D7481 to calculate the Hausner ratio.

Since moisture can affect the flowability of the powder, all powders used in this study were heated within a sample oven (80^0C) to reduce the humidity until the relative humidity was less than 0.01% (measured by A&D MS-70 moisture analyser) before put inside the processing chamber, which has a strict humidity controlled environment.

2.4 Finishing parts quality comparison

Tensile test specimens with a gauge length of 25mm and thickness of 3mm, designed according to ASTM E8-09, were built using a commercial Selective Laser Melting workstation 'MCP SLM-Realizer 100' developed by MCP-HEK Tooling GmbH, which is equipped with a 50W

continuous wave fibre laser with a beam diameter down to 0.026mm. For each brand's powder, five groups of specimens were built using five different scanning speeds: 100mm/s, 150mm/s, 200mm/s, 250mm/s and 300mm/s. Another five groups of specimens were built with five different laser beam diameters (measured using a camera based laser beam profiler) 0.026mm, 0.028mm, 0.030mm, 0.035mm, 0.048mm. Within each group the processing parameters were same for all 5 specimens; the building chamber had an Argon atmosphere, which enabled an oxygen content of less than 0.1%. Laser beam diameter and scanning speed can be parameterised into a laser energy density using the equation above, and these are shown for each experiment in in Tables 1 and 2.

Scanning speed variation	
Laser power	50W
Laser beam diameter	0.028mm
Scanning speed	100mm/s, 150mm/s, 200mm/s, 250mm/s, 300mm/s
Layer thickness	0.05mm
Hatch distance	0.08mm
Scanning strategy	One scan each layer
Pre-heating substrate	Non

Table.1 Specimens built parameters using different scanning speeds

Laser beam diameter variation	
Laser power	50W
Laser beam diameter	0.026mm, 0.028mm, 0.030mm, 0.035mm, 0.048mm
Scanning speed	200mm/s
Layer thickness	0.05mm
Hatch distance	0.08mm
Scanning strategy	One scan each layer
Pre-heating substrate	Non

Table.2 Specimens built parameters using different laser beam diameters

Final part density was measured by cross sectioning specimens and examining the porosity using an optical microscope. Five cross sections were examined to obtain average density value for each sample. Surface roughness was measured by Talylor Hobson Form Talysurf 50. Tensile strength (UTS) and elongation at break were tested using an Instron 3369 and hardness was measured using a Rockwell hardness testing machine (Avery 6402).

3 Results and discussions

3.1 Particle shape, size and size distribution

Particle shapes examined by SEM are shown in Figure.2. Both the SO and the LPW powder appear to be close to spherical with smooth surfaces. Visual inspection suggests that the SO powder consists of a wider range of particle sizes than the LPW.
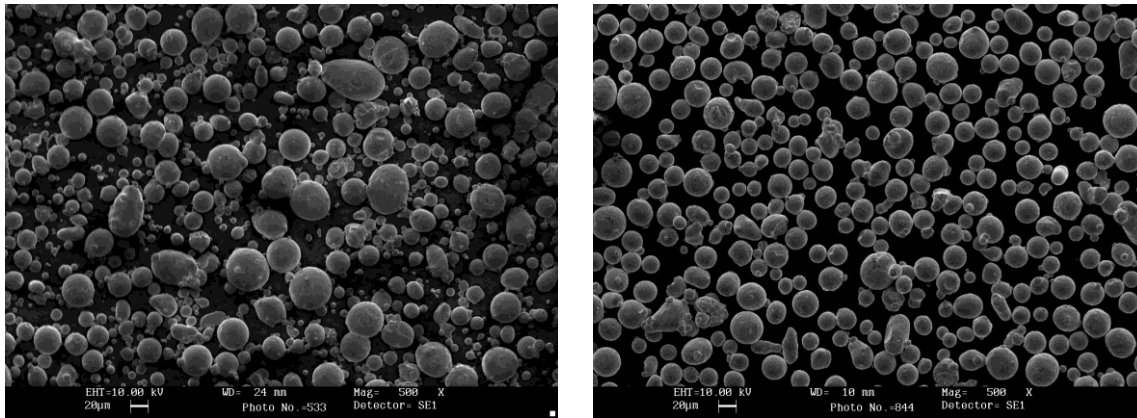

Figure.2 Left-Osprey, right-LPW powder under SEM, mag=500

Measured particle size distributions of SO and LPW powders are shown in Figure.3. The clearly, the two powders have a distinctly different distribution. The SO powder has a wider range and contains significantly more fine particles (<10µm). The mean sizes are close, 27.533µm (SO) and 29.294µm (LPW).
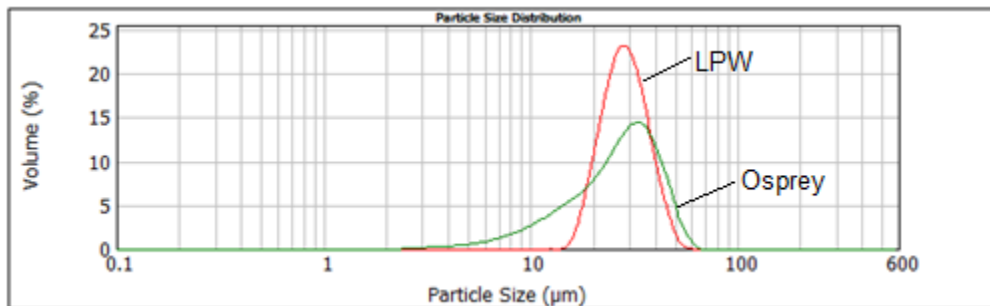

Figure.3 Particle size distribution measured by Mastersizer 2000

3.2 Powder bed density and powder flowability

Apparent density, powder bed density and tapped density of the powders are shown in Table.3. A wider range of particle sizes usually allows a higher density to be achieved as the smaller particles can fit in the gaps between the larger particles and this is reflected in the generally

higher bed density observed for the SO powder. This is likely to be beneficial for the final part. However, the higher density will result in great friction and more possibilities for particles to "lock" together during flow, and thus reduced flowability is seen for the SO powder, shown in Table 4.

Brand	Apparent density (g/ml)	Powder bed density (g/ml)	Tapped density (g/ml)
Osprey	4.54	5.312	5.54
LPW	4.33	4.88	5.03

Table.3 Measured apparent density, powder bed density and tapped density

Brand	Hausner ratio
Osprey	1.22
LPW	1.16

Table.4 Measured powder flowability

3.3 Density of the finishing parts

Scanning Speed	100mm/s	150mm/s	200mm/s	250mm/s	300mm/s
Osprey	99.45%	99.93%	99.55%	99.37%	99.30%
LPW	99.85%	99.65%	99.02%	97.91%	97.22%

Table.5 Average density of parts built using different scanning speeds

Table 5 shows the measured density of the final parts, as a percentage of the full density, i.e., the density achievable with zero porosity. Generally a downward trend in density is observed with increasing scanning speed, reflecting the reduced energy input into the material [12-14]. In addition, the LPW, which was previously observed to have a lower powder bed density, is typically found to have a lower part density than the SO parts, suggesting a possible link between the powder bed density (and thus the particle size distribution) and the final part density. Typical cross-sections of the samples are shown in Figure.4. There is a small drop in average density for SO parts from 150mm/s to 100mm/s with even more energy delivered, and can be caused by fine particles vaporise due to the high temperature generated on the powder bed [13].
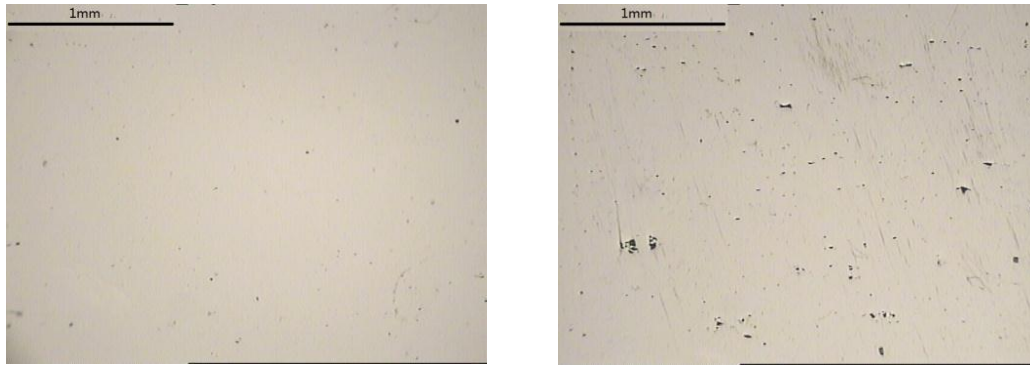
Figure.4 Cross section of parts built on 300mm/s, left-Osprey, right-LPW

Table 6 shows the average density of parts built using five laser beam diameters.

Beam diameter	0.026mm	0.028mm	0.030mm	0.035mm	0.048mm
Osprey	99.90%	99.55%	99.45%	99.26%	98.53%
LPW	99.93%	99.02%	98.63%	97.98%	96.72%

Table.6 Average density of parts built using different laser beam diameters

A similar trend is observed for laser beam diameter. As the diameter is increased, then for the same power, the density tends to decrease. This reflects the same trend in the energy intensity as the beam diameter is increased or the scanning speed increased. Same trend was observed for samples built under different scanning speeds: the Osprey samples perform better than LPW's when using larger laser beam diameters. Again, the LPW parts are typically found to have a lower part density than the SO parts.

3.4 Surface roughness of the finishing parts

Figure 5 and Figure 6 show measured side and top surface roughness R_a for both SO and LPW parts.
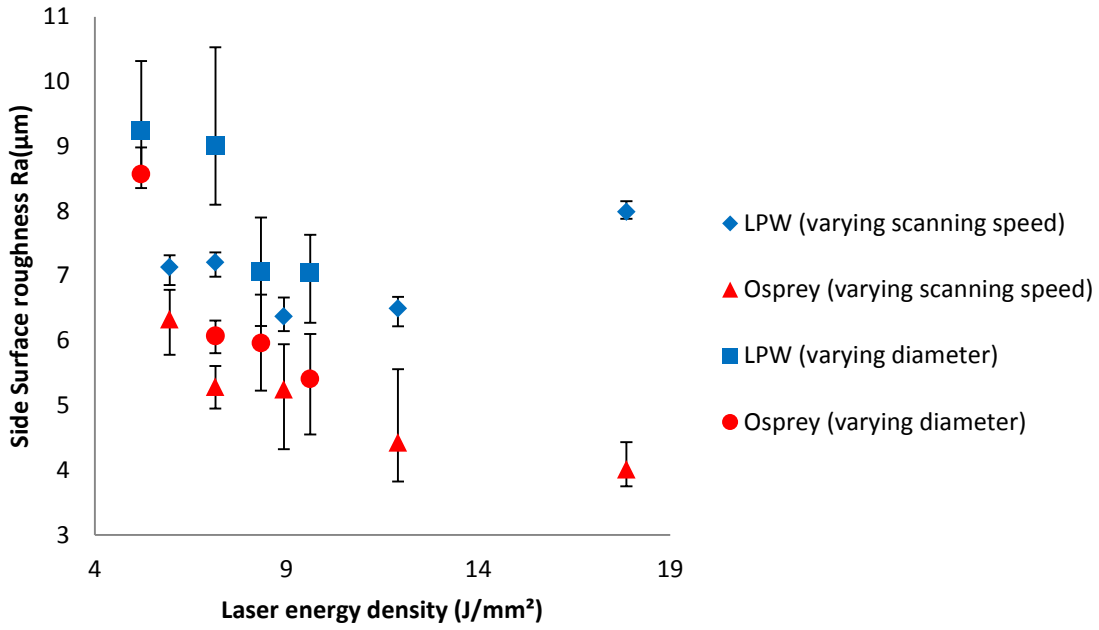
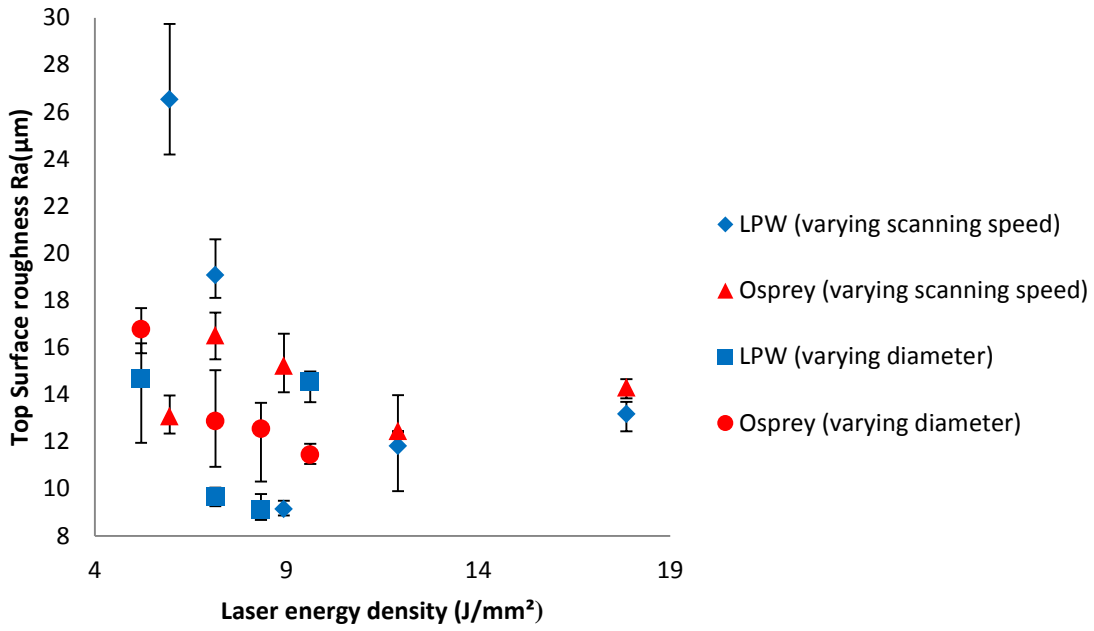*Figure.5 Side surface roughness for both SO and LPW parts*

Figure.6 Top surface roughness for both SO and LPW parts

The results for roughness are more confused. There are suggestions of an increase in roughness as the laser energy intensity is decreased, though there is some significant variation from this, particularly for the top surface roughness of parts built using both SO and LPW powder.

SO parts have better side surface finishing than LPW parts, suggesting a possible link between the particle size distribution and the final parts side surface finishing.

Top surface is usually rougher than side surface on SLM built parts, as can be seen from Figure 5 and 6. Lowest R_a of top surface was observed between the input laser energy density from 7J/mm^2 to 10J/mm^2 for both SO and LPW parts. Higher energy intensity input introduced rougher top surface due to high thermal stresses and non-uniform solidification rate across the powder bed. Top surface roughness of SO parts varies in smaller range compared with LPW parts.

3.5 Tensile strength and elongation of the finishing parts

Figure 7 and Figure 8 show Ultimate Tensile Strength (UTS) and elongation at failure of the samples built using both SO and LPW powders.
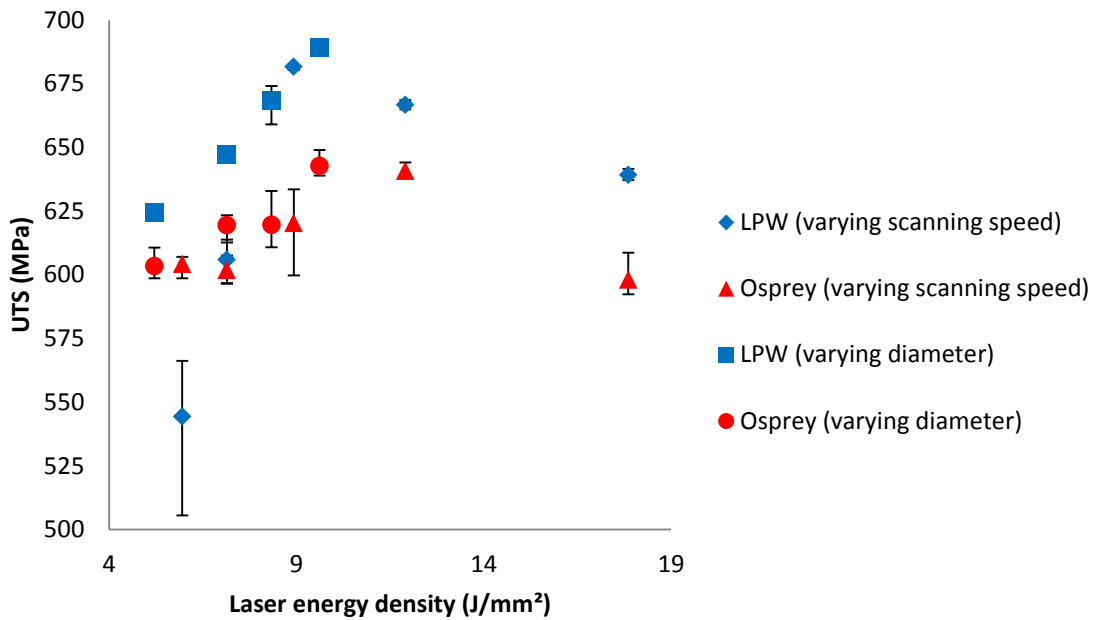

Figure.7 UTS of both SO and LPW parts

Both SO and LPW parts experienced a first increase and then decrease in UTS with increasing the laser energy density. Observed from Figure 7, LPW parts have higher tensile strength than SO parts. A drop in UTS under higher energy intensity input was also observed for both SO and LPW parts.
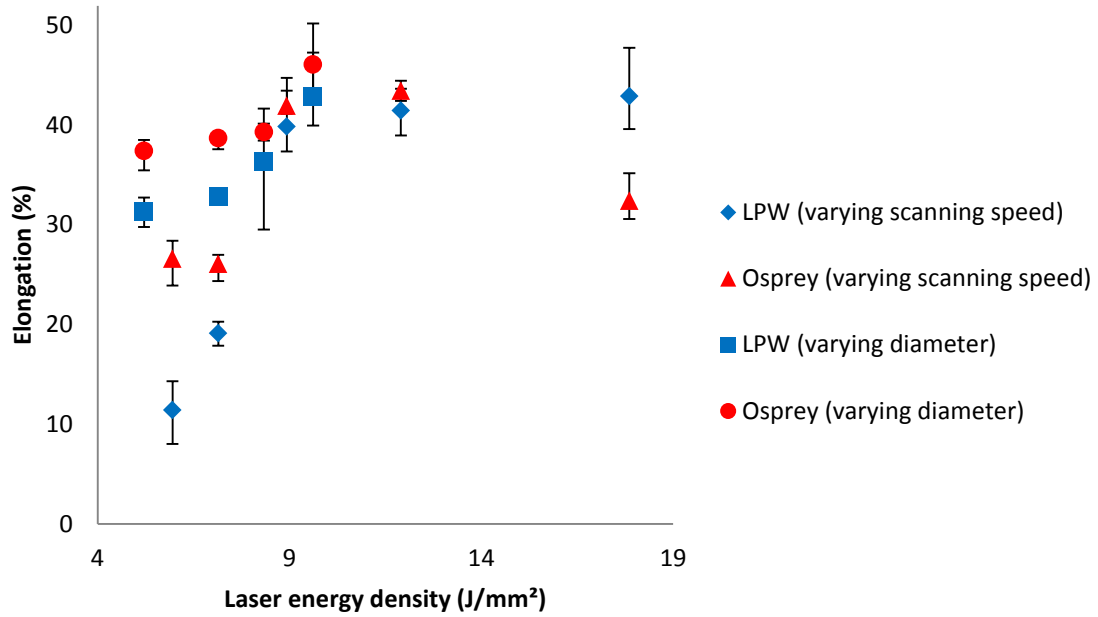
Figure.8 Elongation of both SO and LPW parts

The results for elongation show the similar trend as UTS of both SO and LPW parts, except for LPW parts under high laser energy density. SO parts have higher elongation than LPW parts in most energy intensity, as can be seen from Figure 8.

3.6 Hardness of the finishing parts

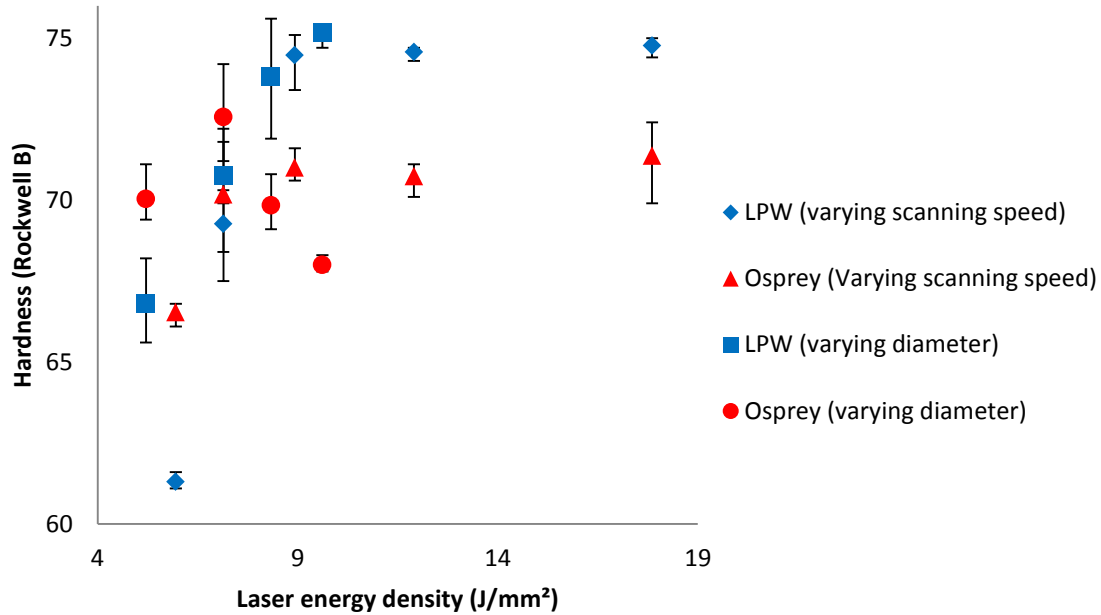Figure.9 shows measured Rockwell B hardness of both SO and LPW parts.

Figure.9 Hardness under different scanning speeds

The results for hardness are more confused. These are suggestions of an increase in hardness as the energy intensity is increased, although there is significant variation for parts using SO powder. Rockwell B hardness of SO parts stayed in a small range between 68 and 72, but didn't form a clear trend under different laser energy density, observed from Figure 9. LPW parts have larger hardness than SO parts when high energy intensity was delivered.

4 Summary conclusions

Powders with different particle size distribution behave differently in selective laser melting process, and introduce differences in powder bed distribution and built part's quality.

Powder with wider range of particle size provides higher powder bed density, generates higher density parts under low laser energy intensity, and generates smoother side surface finishing parts.

Powder with narrower range of particle size provides better flowability, generates parts with higher UTS and larger hardness.

References

[1] J.J. Beaman, J.W. Barlow, D.L. Bourell, R.H. Crawford, H.L. Marcus, K.P. McAlea, Solid Freeform Fabrication: A New Direction in Manufacturing, Kluwer Academic Publishers, 1997.

[2] L. Lu, J. Fuh, Y.S. Wong, Laser Induced Materials and Processes for Rapid Prototyping, Kluwer Academic Publishers, 2001, ISBN: 0792374002.

[3] R.Hague, S. Mansour and N. Saleh, Material and design considerations for Rapid Manufacturing. International Journal of Production Research, 42(22), 2004, 4691.

[4] Randall M. German, Powder Metallurgy Science – 2nd Edition, Metal Powder Industries Federation, 1994, ISBN: 1878954423.

[5] M.J. O'Hara, I.B. Cutler, Sintering Kinetics of binary mixtures of alumina powders. Proceedings of the British Ceramic Society, 12, 1969, pp.145-154.

[6] H.M. Lee, C.Y. Huang, C.J. Wang, Forming and sintering behaviours of commercial α-Al_2O_3 powders with different particle size distribution and agglomeration, Journal of materials processing technology, 209, 2009, pp.714-722.

[7] Baoshan Li, Guorong Li, WangZhong Zhang, AiLi Ding, Influence of particle size on the sintering behaviour and high-power piezoelectric properties of PMnN-PZT ceramics, Materials science and engineering, B 121, 2005, pp.92-97.

[8] Ken Darcovich, Floyd Toll, Pierre Hontanx, Virginie Roux, Kazunari, Shinagawa, An experimental and numerical study of particle size distribution effects on the sintering of porous ceramics, Materials science and engineering, A 348, 2003, pp.76-83.

[9] J.S. Chappell, T.A. Ring, J.D. Birchall, Particle size distribution effects on sintering rates, Journal of Applied Physics, 60 (1) 1986, pp.383-391.

[10] T.S. Yeh, M.D. Sacks, Low-temperature sintering of aluminium oxide, Journal of the American ceramic society, 71 (10) 1988, pp.841-844.

[11] http://en.wikipedia.org/wiki/Hausner_ratio

[12] T.H.C. Childs, Raster scan selective laser melting of the surface layer of a tool steel powder bed. Proc. IMechE, 219(B), 2005, pp.109-115.

[13] J.P. Kruth, P. Mercelis, J.V. Vaerenbergh, L. Froyen, M. Rombouts, Binding mechanisms in selective laser sintering and selective laser melting, Rapid Prototyping Journal, 11(1), 2005, pp.26-36.

[14] R. Morgan, C.J. Sutcliffe, W. O'Neill, Density analysis of direct metal laser re-melted 316L stainless steel cubic primitives, Journal of Materials Science, 39(4), 2004, pp.1195-1205.